Ionization of positive argon ions by electron impact

E. D. Donets and A. I. Pikin

Joint Institute for Nuclear Research
(Submitted October 28, 1975)
Zh. Eksp. Teor. Fiz 70, 2025–2034 (June 1976)

The "Krion" electron-beam source has been used to determine the ionization cross sections of argon ions between Ar^{+4} and Ar^{+12} at incident-electron energies $\sim 2.5 \pm 0.15$ keV. The cross sections were obtained by comparing theoretical calculations with the spectrum of charge states of the ions as functions of the time of interaction with the electron beam. To achieve satisfactory agreement between the calculated and measured results, the theoretical model of ionization must include both single-electron and two-electron ionization in a single collision for the ions Ar^{+5} and Ar^{+6}. This procedure was used to obtain the following total and partial ionization cross sections (in units of 10^{-18} cm^2): $\sigma_4 = 4.6$; $\sigma_5 = 3.5$ ($\sigma_{5\to6} = 2.05$; $\sigma_{5\to7} = 1.45$); $\sigma_6 = 2.3$ ($\sigma_{6\to7} = 0.92$; $\sigma_{6\to8} = 1.38$); $\sigma_7 = 1.4$; $\sigma_8 = 0.88$; $\sigma_9 = 0.65$; $\sigma_{10} = 0.45$; $\sigma_{11} \sim 0.30$; $\sigma_{12} \sim 0.20$. The uncertainties in these values amount to $\pm 15\%$. The experimental ionization cross sections are compared with calculated values.

PACS numbers: 34.70.Di

1. INTRODUCTION

Studies of the ionization of positive ions of different elements by electron impact are of considerable interest because they may yield basic information on the electron shells of ions when measurements are made of the probabilities of the various processes involving the participation of both the incident electron and the shell electrons in ions of different charge.

Moreover, the ionization cross sections of positive ions have direct applications in plasma physics, the development of sources of multiply-charged ions, in astrophysical studies, and so on.

Measurements of the cross section for the ionization of positive ions by electron impact are traditionally carried out by crossing ion and electron beams.[1] With all its advantages, this method suffers from relatively low sensitivity which prevent its application to the investigation of more than two or three stages of the successive ionization process.

Other and more sensitive methods have been developed in recent years, including, in particular, the ion trap method.[2-5] A cryogenic variant of the "Krion" electron-beam ion source has been developed at the High-Energy Laboratory of the Joint Institute for Nuclear Research.[6] It has been found to be a sufficiently effective instrument for the determination of cross sections for the ionization of positive ions by electron impact, right up to ions with only the inner electron shells still present. For some light elements, it has been possible to determine the separation cross section even for the last electron in the K shell.[7]

In this paper, we give a description of the experimental arrangement, and report some experimental data on the ionization of positive argon ions interacting with electrons with a fixed energy $\sim 2.5 \pm 0.15$ keV.

2. EXPERIMENTAL ARRANGEMENT

Figure 1a shows the inner part of the "Krion" source incorporating a time-of-flight mass spectrometer. The electron beam emitted by the cathode 1 of the electron gun (1, 2) is focused by the solenoid 3 and, after leaving the magnetic field, is recorded by the collector 4 to which the beam electrons are drawn by the field of the extracting electrode 5. The sections of the drift tube 6 are designed to produce the required distribution of potential in the beam-drift space. The magnetic pole piece 7 produces the necessary magnetic-field configuration at exit from the solenoid. The source 8 of the working medium is located in the region of the third section of the drift tube.

To ensure that the time of interaction between the ions and the electron beam is long enough, an electrostatic ion trap is produced in the ionization region. This ensures that the escape of ions in the radial direction is restricted by the electron-beam space-charge field, whereas, in the axial direction, the ions are contained by the potential barriers produced by the end sections of the drift tube.

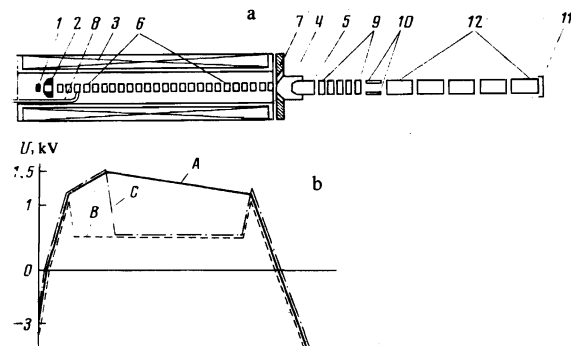The ion source is pulsed at a rate of 1 cycle per sev-

FIG. 1. a) Interior of the Krion source incorporating the time-of-flight mass spectrometer (TFMS): 1—electron gun cathode; 2—electron gun anode; 3—focusing solenoid; 4—electron collector; 5—extracting electrode; 6—drift-tube sections of the ion source; 7—magnetic pole; 8—source of working material; 9—set of electrostatic lenses; 10—mass-spectrometer modulator; 11—ion collector of mass spectrometer; 12—drift tubes of mass spectrometer. b) Potential distributions A, B, C along the drift tube of the ion source.
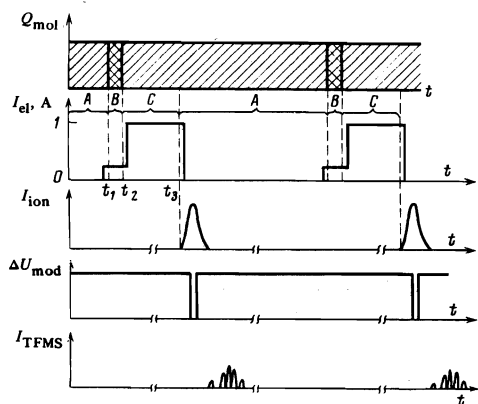
FIG. 2. Time diagram for the processes in the Krion source and the mass spectrometer. Q_{mol}—flux of molecules of working material in the drift tube of the ion source; I_{el}—electron current generated by the gun; I_{ion}—ion current at exit from the source; ΔU_{mod}—potential difference across the plates of the modulator in the mass spectrometer; I_{TFMS} current from the ion collector of the mass spectrometer (recorded ion-charge spectrum).

eral seconds. The sequence of the various processes is illustrated by Figs. 1b and 2.

The source of the working material produces a constant-intensity flux of molecules in the drift tube. Initially, the electron-beam density is low and the distribution of potentials over the sections (Fig. 1b, A) is such that all the ions leave the electron beam in the axial direction. While the electron-beam density is low, the potential distribution B is applied to the sections at time t_1. The point of intersection of the molecular and electron beams is then located inside the electrostatic ion trap. From this moment onward, all the ions of the working material produced in the beam are captured by the trap and are uniformly distributed throughout the volume of the electron beam between the axial potential barriers. The accumulation of the ions of the working material continues during the adjustable time $t_2 - t_1$ which is determined by the flux of molecules of the working material, the energy of the beam electrons, and the required degree of compensation of the electron-beam space charge by the ion charge at the end of the ionization process.

When a sufficient amount of ions of the working material has accumulated in the trap, the potential distribution C is applied to the sections of the drift tube at time t_2. The left-hand edge of the electrostatic trap is then shifted so that the point of intersection between the molecular and electron beams, which is located in the region of the axial potential gradient, is separated from the trap by a potential barrier. All the newly formed ions of the working material then escape in the direction of the electron-gun cathode, and do not reach the trap.

This method of injecting the working material into the electrostatic trap, the so-called "electron regulation method," was proposed in[8] and is realized for the first time in the "Krion" source. Since it is based on pulsed injection, the electron regulation method can be used to vary the amount of working material introduced

into the ionization region within very broad limits because the time of injection can be varied between tens of milliseconds and tens of microseconds. Experiments have shown that the working material does not enter the trap after the end of the injection process. The above method has been tested with the following working gases: ethylene, nitrogen, neon, argon, xenon, and helium. The ionization process is accompanied by an increase in the ion space charge and in the amplitude of ion radial oscillations. To ensure that this does not lead to a loss of ions, the electron-beam density is increased during the ionization process, and this results in a reduction in the amplitude of these radial oscillations.

When the residual gas is presented in the ionization region, the time of interaction between ions and the electron beam is determined by the rate of compensation of the electron-beam space charge by the space charge due to the residual-gas ions. Under our conditions, the residual gas pressure in the ionization region was $\sim 2 \times 10^{-11}$ Torr and, at the end of the 40-millisecond ionization, the background in the total ion charge was not more than 10%. The maximum time of interaction between the ions and the electron beam is equal to the length of the electron pulse (40 msec), i.e., it is restricted by the technological possibilities of the supply systems for the electron gun. If there were no such restrictions, then with the existing background level, complete compensation of the electron charge by the ions would occur in about 0.5 sec.

When the ionization process is over, the initial distribution of potentials (A) is re-established and all the ions stored up in the trap are extracted for analysis. The length of the ion-current pulse is determined by the time taken to replace the potential distribution C by the distribution A. This time can be varied between 40 and 500 μsec.

The ion-charge analysis is carried out by a time-of-flight mass spectrometer (Fig. 1a) with a path length of 1m. Ions accelerated by the field of the extracting electrode pass through the set of electrostatic lenses 9 and eventually enter the capacitor-type modulator 10. A constant potential difference is applied between the plates of this modulator, and this deflects the ions so that the ion beam is not recorded at the exit from the mass spectrometer. While the ions are being extracted from the source, the potential difference between the capacitor plates is reduced to zero for a short time ($\sim$100 nsec), and an ion packet is allowed to pass through toward the recording system. The flight-time separation of the ions in the drift space then occurs in accordance with their charges, and the ion collector of the mass spectrometer records the ion-charge spectrum. To ensure that the recorded spectra provide information about all the ions extracted from the source, a series of electrostatic lenses formed by the drift tubes 12 and held at different potentials is inserted into the ion drift space so that the ion collector receives practically all the ions leaving the source in the absence of the potential difference between the modulator plates.

By applying the equalizing signal to the plates of the

modulator of the mass spectrometer at different instants of time relative to the beginning of the transition from the potential distribution C to the distribution A, it is possible to examine the charge composition of different parts of the ion-current pulse. It turns out that, for short ion-current pulses ($\sim 40-60$ sec), the beginning of the pulse is somewhat richer in highly charged ions than its end, and this may be due to the higher mobility of high-charge ions. However, we may suppose with reasonable justification that the charge composition of the central part of the pulse is characteristic of the ion-charge pulse as a whole.

A detailed description of the design of the "Krion" source, including its cryogenic and magnetic systems, the formation of the electron beam, and other features is given in[6,9].

3. MEASUREMENT RESULTS AND DETERMINATION OF THE IONIZATION CROSS SECTIONS

The process of ionization of positive argon ions was investigated experimentally as follows. A certain amount ($\sim 10^{10}$) of argon ions was initially introduced into the electron beam of the "Krion" source for periods of about $100-150$ μsec. At the end of this period, which was, in fact, the ionization time, the ions were extracted from the electron beam and analyzed in accordance with their times of flight. The charge spectrum of ions corresponding to the given ionization time was recorded on the screen of the S1-42 oscillograph. The ionization time was then altered, and the associated change in the charge spectrum was recorded.

Figure 3 shows typical charge spectra for argon ions corresponding to ionization times of 5, 10, and 20 msec. The beam electrons had energies of ~ 2.5 keV, and the beam current was 1 A. As can be seen, since pulsed injection of the working material into the electron beam was employed, the ions with the lower charges were gradually "burnt up," and ions of higher charge appeared in the spectrum. At the same time, the residual-gas background was small and did not exceed 10% even at the maximum ionization time used in these experiments (~ 40 msec).

The principle of operation of the electron-beam ion source shows that the total number of elementary charges carried by all the ions at any time within the ionization interval cannot be greater than the number of fast electrons in the beam, the space charge of which retains the ions. Two situations can therefore arise: 1) at the initial instants of time, and depending on the length of the ionization period, different amounts of low-charge ions are introduced into the beam in such a way that, at the end of the ionization process, the same maximum possible total ion space charge is accumulated independently of the length of the ionization process, and this charge is roughly equal to the space charge due to the fast electrons, and 2) each time, and independently of the period of ionization, the same amount of low-charge ions is introduced into the beam in such a way that the ion and electron space charges become equal only for a given maximum duration of ionization.
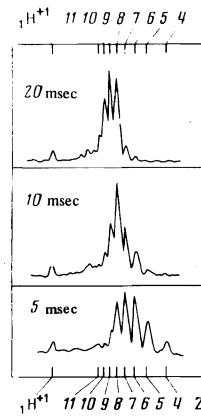

FIG. 3. Argon-ion charge spectra corresponding to ionization times of 5, 10, and 20 msec.

Either situation is acceptable for studies of ionization with the only difference that, in the first case, the total ion charge is constant whereas, in the second, the total number of ions is constant.

We prefer to use the first situation because the sensitivity is then higher and this is important for short ionization periods when the number of lines in the charge spectrum is large. The processing of the spectrum corresponding to a given ionization time involves the determination of the areas under the peaks corresponding to the different charges, the determination of the number of ions of given charge in relative units, and, finally, the determination of the ion-charge distribution normalized to unity. The determination of these distributions as functions of the ionization time yields the time evolution of the charge spectra, which is particularly convenient for the determination of the ionization cross sections.

It is clear that the case of successive ionization, when only one orbital electron is removed in each event, is mathematically analogous to the disintegration of radioactive material which, after a number of disintegrations, eventually ends in a stable species. The analog of this, in our case, is a bare nucleus without any electrons around it. A description of this process is given, for example, in Segre's book.[10] In our case, the radioactive decay constant is analogous to the ionization cross section, and the time is analogous to the product of the electron-beam flux density j and the ionization time τ.

The electron-beam density was determined as an average over the beam and is given by $j = 6.2 \times 10^{18} I / S_k$, where I is the electron-beam current in amperes and S_k is the area of the electron-gun cathode in cm². This formula is valid because we have used an electron gun in a magnetic field of about 1.2 T, so that the area of the electron beam corresponding to as high a perveance as $\sim (8-10) \times 10^{-6}$ A/V$^{3/2}$ can be assumed to be equal to the area of the emitting surface of the cathode for voltages of $\sim 2-3$ kV.

Figure 4 shows the charge spectra of argon ions for different $j\tau$. The experimental points represent the number of ions of given charge (n_z) with the total number of ions normalized to unity. We have investigated the ionization of argon between Ar^{+4} and Ar^{+12} with $j\tau$ in
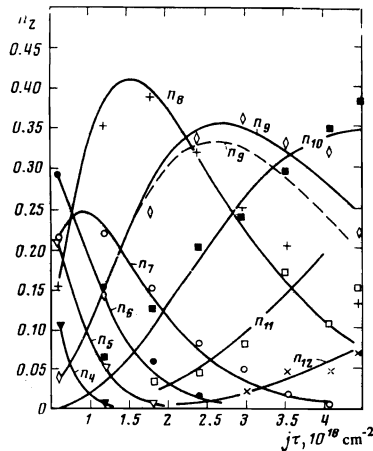
E. D. Donets and A. I. Pikin   1059

FIG. 4. Evolution of the charge spectrum in the case of argon ions: ▼—+4, ▽—+5, ●—+6, ○—+7, +—+8, ◇—+9, ■—+10, □—+11, ✕—+12.

the range between 0.6×10^{18} and 4.5×10^{18} cm^{-2}.

According to[10], the solution of the kinetic equations for the number of ions $n_k(j)$ of given charge k in the case of successive ionization is
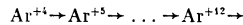
$$n_k(j\tau) = A_{k1}e^{-\sigma_1 j\tau} + A_{k2}e^{-\sigma_2 j\tau} + \ldots + A_{kk}e^{-\sigma_k j\tau}$$

where

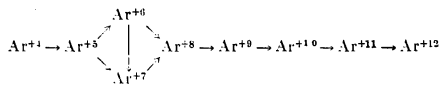$$A_{k,i} = A_{k-1,i}\sigma_{k-1}/(\sigma_k - \sigma_i) \text{ and } n_k(0) = A_{k1} + A_{k2} + \ldots + A_{kk},$$

and σ_i is the cross section for the ionization of an ion of charge i into an ion of charge $i+1$.

We have tried to fit the experimental data on the ionization cross sections for the chain

$$Ar^{+4} \to Ar^{+5} \to \ldots \to Ar^{+12} \to$$

(i.e., assuming that only one electron ionization occurs at each stage) to theoretical curves. However, this was not possible. To achieve satisfactory agreement between the calculated and experimental curves $n_i(j\tau)$, it is essential to assume that both one-electron and two-electron ionization occurs in the Ar^{+5} and Ar^{+6} ions.

Figure 4 shows the calculated $n_i(j\tau)$ curves for the following ionization chain:

$$Ar^{+4} \to Ar^{+5} \begin{array}{c} \nearrow Ar^{+6} \searrow \\ | \\ \searrow Ar^{+7} \nearrow \end{array} Ar^{+8} \to Ar^{+9} \to Ar^{+10} \to Ar^{+11} \to Ar^{+12}$$

and the following set of total and partial ionization cross sections (in units of 10^{-18} cm^2):

$$\sigma_4 \sim 4.6,$$
$$\sigma_5 = 3.5 \ (\sigma_{5\to6} = 2.05, \quad \sigma_{5\to7} = 1.45),$$
$$\sigma_6 = 2.3 \ (\sigma_{6\to7} = 0.92, \quad \sigma_{6\to8} = 1.38),$$
$$\sigma_7 = 1.4, \quad \sigma_8 = 0.88, \quad \sigma_9 = 0.65,$$
$$\sigma_{10} = 0.45, \quad \sigma_{11} \approx 0.30, \quad \sigma_{12} \approx 0.20.$$

For Ar^{+7} and ions of higher charge, the two-electron

ionization need not be introduced with the existing precision of experimental results. In the case of Ar^{+4}, the experimental results are not inconsistent with the presence of two-electron ionization with $\sigma_{4-6} \sim 1.5 \times 10^{-18}$ cm^2 but there is not enough information about the burn-up of these ions, and the rate of burn-up as compared with other ions is high for the relatively low initial number of Ar^{+4} ions. This means that the introduction of two-electron ionization of Ar^{+4} has a slight effect on the subsequent dynamics of the spectra and, insofar as the analysis of experimental results is concerned, the inclusion of this process is not essential. Physically, however, this process must, of course, be admitted.

To illustrate the agreement between the experimental and calculated data (for the above choice of ionization cross sections), the function $n_9(j\tau)$ is also shown for σ_9 increased by 12% (broken line in Fig. 4). We estimate that our cross sections are accurate to within $\pm 15\%$. This uncertainty is determined both by the experimental method itself and by the possible incompleteness of the theoretical ionization model.

Figure 5 shows the total ionization cross sections (σ), the one-electron cross sections ($\sigma_{(1)}$), and the two-electron cross sections ($\sigma_{(2)}$) as functions of the ion charge.

4. DISCUSSION OF EXPERIMENTAL RESULTS

In the usual notation, the electron-shell configuration of the argon atom is $1S^2 2S^2 2P^6 3S^2 3P^6$. Carlson et al.[11] have reported the electron-subshell configurations and the calculated ionization potentials for all the argon ions. It follows from their data that, in our case (incident-electron energy of 2.5 keV), all electrons can participate in the ionization process with the exception of K-shell electrons.

A. Two-electron ionization

It is natural to suppose that two-electron ionization of Ar^{+4}, Ar^{+5}, and Ar^{+6} in a single collision is the result of the appearance of vacancies in the L shell when one of the L electrons is either transferred to the continuous spectrum or to one of the higher-lying levels. Many authors and, in particular, Salop,[12] consider that, when vacancies appear in the L shell and there are two or more electrons in the M shell, the probability of two-electron ionization is 100%, whereas one-
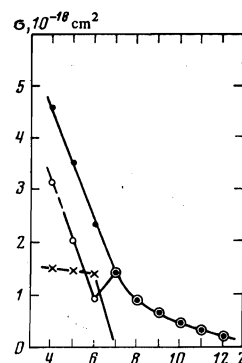

FIG. 5. Ionization cross section of argon ions as a function of the ion charge [σ—total cross section (●), σ_1—one-electron ionization cross section (○), σ_2—two-electron ionization cross section (✕)].
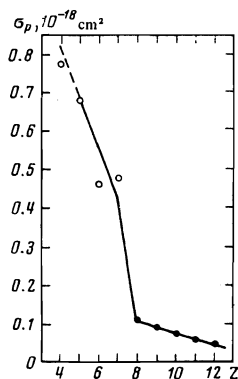
FIG. 6. One-electron ionization cross section (per shell electron) of argon ion as a function of ion charge: ○— M-shell, ●—L-shell.

electron ionization must predominate in the Ar^{+7} ion because of the corresponding selection rules. Our result can therefore be looked upon as experimental confirmation of these theoretical predictions. Moreover, experiment also yields the relative probabilities and absolute cross sections for the appearance of vacancies in the L shell of Ar^{+6} with the transition of the L electron separately to the continuous spectrum and to higher-lying excited states.

In fact, the measured ionization cross section of Ar^{+8}, which has a complete set of L electrons, is 0.88×10^{-18} cm^2. For Ar^{+6}, the cross section for the removal of an electron from the L shell to the continuous spectrum can be assumed to be close to this value. The correction is due to the fact that the binding energy of the 2s and 2p electrons in Ar^{+6} is somewhat lower than in Ar^{+8}. We have no data at present on the electron binding energies in argon-ion subshells. However, Hahn and Watson have shown theoretically[13] that, for Ca^{+8} and Ca^{+10}, this energy difference is about 10%. Accordingly, using the well-known energy dependence of the ionization cross section, we obtain a ~10% correction. Thus, the cross section for two-electron ionization, which is the result of the transition of one of the L electrons in Ar^{+6} to the continuous spectrum, is ~0.96 $\times 10^{-18}$ cm^2, and the corresponding figure for the transition to an excited state is ~0.42×10^{-18} cm^2. To what extent this result is acceptable from the theoretical standpoint will be indicated by subsequent research.

The somewhat higher value of the two-electron ionization cross section of the Ar^{+5} ion corresponds to the further reduction in the L-electron binding energy as compared with Ar^{+6}.

B. One-electron ionization

Since for the $Ar^{+4,5,6}$ ions the removal of an electron from the L shell leads to two-electron ionization, the one-electron ionization cross section of these ions includes contributions due to 3P and 3S electrons. The fact that $\sigma_{6-7} < \sigma_{6-8}$ is connected with this result, which means that, for the given incident electron energy, the probability of ejecting an electron from a closed L shell is greater than the corresponding figure for the M shell which, in the case of Ar^{+6}, contains two 3S electrons.

Moreover, if we suppose that the cross section for the removal of an electron from the L shell of Ar^{+7} is

roughly equal to the ionization cross section of Ar^{+8}, then the cross section for the removal of the last 3S electron becomes known. It is thus possible to determine the partial cross section σ_p per M- and L-shell electron in ions of the corresponding charge. Figure 6 shows σ_p as a function of the ion charge. It is clear that this cross section falls smoothly within a given shell, but then undergoes a discontinuous change between the M and L shells, in accordance with the change in the ionization potentials.

The partial cross sections per nl-electron are usually calculated from the Bethe formula[12]

$$\sigma_{nl} = \frac{K}{E_i I} \ln \frac{E_k}{I},$$

where K is a constant, E_k is the kinetic energy of the electrons, and I is the electron binding energy in the corresponding nl-subshell.

The values of K obtained from the best agreement between the experimental and calculated cross sections for one-electron ionization are as follows:

Z:	4	5	6	7	8	9	10	11	12
$K, 10^{-14} eV^2 \cdot cm^2$:	4.62	5.15	5.27	6.30	5.92	6.40	6.64	6.58	6.65

It is clear that $K = 6 \times 10^{-14}$ $eV^2 \cdot cm^2$ can be successfully used to calculate the ionization cross sections for ions at the present level of accuracy. This value is close to that reported previously by Lotz[14] ($K = 4.5 \times 10^{-14}$ $eV^2 \cdot cm^2$).

5. CONCLUSIONS

The most interesting development of the present work would be the determination of the energy dependence of measured cross sections with maximum possible accuracy of experimental results, and the extension of these studies to the ions $Ar^{+1}-Ar^{+3}$ and $Ar^{+13}-Ar^{+17}$. The complete realization of this program is possible, but would require higher beam densities than can be obtained with the "Krion" source.

[1] J. B. Hasted, Physics of Atomic Collisions, Butterworths, London, 1964 (Russ. Transl., Mir, M., 1965, p. 337).
[2] F. A. Baker and J. B. Hasted, Philos. Trans. R. Soc. London 261, 33 (1966).
[3] P. A. Redhead, Can. J. Phys. 45, 1791 (1967).
[4] P. A. Redhead, Can. J. Phys. 48, 1906 (1970).
[5] P. A. Redhead and G. P. Gopalaram, Can. J. Phys. 49, 585 (1971).
[6] E. D. Donets and A. I. Pikin, Zh. Tekh. Fiz. 42, 2373 (1975) [Sov. Phys. Tech. Phys. 20, 1477 (1976)].
[7] E. D. Donets and V. I. Ilyushchenko, Soobshch. OIYaI R7-8310, 1974.
[8] E. D. Donets, V. I. Ilyushchenko, and V. A. Al'pert, Avtorskoe svidetel'stvo 375708 (Inventor's Certificate 375708), Byulleten' (Bulletin) No. 16, 1973.
[9] V. G. Aksenov, E. D. Donets, A. G. Zel'dovich, A. I. Pikin,

1061   Sov. Phys. JETP, Vol. 43, No. 6, June 1976

E. D. Donets and A. I. Pikin   1061

and Yu. A. Shishkov, Soobshch. OIYaI (JINR Commun.) R8-8563, 1975.

[10] E. Segrè (ed.), Experimental Nuclear Physics, John Wiley, New York, 1959 (Russ. Transl., Vol. 3, IIL, M., 1961, p. 13).

[11] T. A. Carlson, C. W. Nestor, N. Wasserman, and J. D.

McDowell, At. Data 2, 63 (1970).

[12] A. Salop, Phys. Rev. A 9, 2496 (1974).

[13] Y. Hahn and K. N. Watson, Phys. Rev. A 7, 491 (1973).

[14] W. Lotz, Z. Phys. 216, 241 (1968).

Translated by S. Chomet

On Coulomb polarization of vacuum

Ya. I. Granovskii

Donetsk State University
(Submitted January 3, 1976)
Zh. Eksp. Teor. Fiz. **70**, 2035–2040 (June 1976)

The charge density induced by a Coulomb field is represented as the absorptive part of a certain operator, which can be reduced in turn to a finite-rotation operator of the Coulomb dynamic group $O(2,1)$. In this way the total induced charge can be calculated and the cause of suppression of the contribution from higher partial waves can be ascertained.

PACS numbers: 12.20.Ds

INTRODUCTION

The polarization of a vacuum of charged particles by an external electromagnetic field was first considered by Dirac, Heisenberg, Serber, and Uehling in the weak-field approximation.[1] They obtained an expression for the induced charge density

$$\rho = -\alpha \Box \rho_0 / 15\pi m^2 \tag{1}$$

in terms of the charge density ρ_0 that produces the external field.

Subsequently Weisskof and Schwinger[2] presented a general expression suitable for fields of arbitrary strength, but this expression turned out to be too complicated and yielded a result in explicit form only in some particular cases. In addition, the important case of a Coulomb field could not be handled by this method.

Wichmann and Kroll[3] have therefore returned to the direct calculation methods and, by using very complicated computations, obtained corrections to the Uehling formula. These calculations were recently radically improved by Brown *et al.*[4]

The question of the calculation of the Coulomb polarization of vacuum has been under lively discussion in recent times, since this effect turned out to be particularly noticeable in heavy μ-mesic atoms.[5] However, even after the publication of[4], the theory of Coulomb polarization remains rather cumbersome. The reason, in our opinion, is the neglect of the symmetry of the Coulomb field.

We describe below a calculation method that takes into account this important property explicitly.

GENERAL RELATIONS

We first transform the well known formula[2] for the induced current

$$j_\mu = \text{tr}\,\gamma_\mu G, \tag{2}$$

which contains for an electron in the external field, a Green's function satisfying the equation

$$[m - \gamma(p - eA)]G = 1. \tag{3}$$

In operator form ($\Pi = p - eA$) we have

$$j_\mu = \text{tr}\,\gamma_\mu(m - \hat{\Pi})^{-1} = \text{tr}\,\gamma_\mu(m + \hat{\Pi})(m^2 - \hat{\Pi}^2)^{-1} = \text{tr}\,\gamma_\mu\hat{\Pi}(m^2 - \hat{\Pi}^2)^{-1} \tag{4}$$

(the term $\sim m$ has dropped out, since it contains an odd number of Dirac matrices). Transferring $\hat{\Pi}$ to the right, we obtain the expression

$$j_\mu = \text{tr}\,\gamma_\mu(m^2 - \hat{\Pi}^2)^{-1}\hat{\Pi},$$

which when summed with (4) yields

$$j_\mu = \text{tr}\,\Pi_\mu(m^2 - \hat{\Pi}^2)^{-1} = \Pi_\mu \int_0^\infty ds\,\text{tr}\exp\{-s(m^2 - \hat{\Pi}^2)\}. \tag{5}$$

The charge density induced by the static field is equal to

$$\rho_E = (E - eA_0) \int_0^\infty ds\,\text{tr}\exp\{-s[m^2 + p^2 - (E - eA_0)^2 - e\sigma_{\mu\nu}F_{\mu\nu}/2]\} \tag{6}$$

or

$$\rho_E = \frac{1}{2}\frac{d}{dE}\int_0^\infty \frac{ds}{s}\,\text{tr}\exp\{-s[m^2 - \hat{\Pi}^2]\}. \tag{6a}$$

This means that the total charge density is equal to

$$\rho = \int_{-i\infty}^{+i\infty} \rho_E \frac{dE}{2\pi i} = (2\pi i)^{-1}[W(E) - W(-E)]_{E\to i\infty}, \tag{7}$$

so that the problem reduces to the calculation of